TJNN Thai Journal of Nanoscience and Nanotechnology

Enhanced Piezo-Photocatalytic Degradation of Rhodamine B Using Different ZnO Nanostructures Under Xenon Irradiation and Ultrasonic Activation

Suttida Dorweng, Maneerat Songpanit, Kanokthip Boonyarattanakalin and Wanichaya Mekprasart*

School of Integrated Innovative Technology, King Mongkut's Institute of Technology Ladkrabang, Bangkok, 10520, Thailand

Received: 27 May 2025, Revised: 25 June 2025, Accepted: 26 June 2025

Abstract

The contamination of wastewater with synthetic organic dyes has become a significant environmental challenge. To address this issue, zinc oxide (ZnO) has attracted considerable attention due to its non-toxic nature and versatile applications, especially in photocatalytic materials. Enhancing the efficiency of photocatalysis requires reducing electron-hole recombination, which can be achieved through doping or composite formation with other materials. Additionally, the integration of piezoelectric properties presents an effective strategy to enhance ZnO-based photocatalysts, given their excellent piezoelectric characteristics. In this study, the piezo-photocatalysis properties of ZnO nanostructures with spherical, plate-like, and rod-like morphologies were systematically investigated under xenon lamp irradiation coupled with piezo-mechanical stimulation. Rhodamine B (RhB) was employed as a model dye to evaluate photocatalytic performance under various conditions, for example, light irradiation, piezo-assisted activation combined with light irradiation, and the absence of light. The absorbance of the dyes under photocatalytic reaction was then measured using a UV-visible spectrophotometer. The experimental results revealed that the highest dye degradation efficiency was achieved when using rod-like ZnO photocatalyst under combined piezo-assisted and light irradiation. This superior performance can be attributed to its asymmetric geometry, which enhances the generation of an internal electric field on the photocatalyst surface under piezoelectric activation, thereby promoting efficient charge separation. Moreover, the 1D structure of the rod-like facilitates directed electron transport along its longitudinal axis and provides a higher density of active sites, contributing further to their enhanced photocatalytic activity.

Keywords: Piezo-photocatalyst, Xenon irradiation, Zinc oxide, Nanostructures

1. Introduction

The global population is continuously increasing, with an average growth of 200,000 people per day, leading to greater consumption of resources such as housing, clothing, food, medicine, and public health services. Consequently, resource management faces challenges, contributing to various issues, including air pollution from housing construction, waste pollution, food waste, and other residuals from human consumption. Among the most significant pollutants is water pollution, which greatly impacts globally important resources. Water pollution is primarily caused by chemicals and waste released from industrial operations and agriculture, which often include toxic waste, pesticides, and fertilizers [1]. The most prevalent source of wastewater is industrial discharge, followed by community waste, leading to reduced oxygen levels, the presence of pathogens in rivers and canals, and disturbance in aquatic ecosystems, such as foul odors from rotten water. Thus, various approaches have been proposed to address wastewater problems, including waste collection from water sources and chemical treatment methods [2]-[3]. One particularly promising approach is photocatalysis, an effective technique for treating wastewater contaminated with both organic and inorganic substances, including dye-laden water [4]-[5]. This process involves the use of semiconductor materials as a photocatalyst, which is activated by energy greater than its band gap under light irradiation. The generation of electron-hole

Corresponding Author: wanichaya.me@kmitl.ac.th

pairs on its photocatalyst surface plays a key role relating to the degradation mechanism under light activation. Among photocatalyst materials, titanium dioxide (TiO_2) and zinc oxide (ZnO) are considered highly effective due to their high stability, non-toxicity, and low cost [6]-[8]. TiO_2 material is widely used due to its strong oxidizing ability, excellent chemical stability, and biocompatibility. On the other hand, ZnO exhibits high performance in photocatalysis because of its superior electron mobility in the photocatalytic process, although a wider band gap energy compared to TiO_2 is a limitation. Therefore, the enhancements to ZnO photocatalyst have been explored through metal ion doping, morphological tuning, and forming composites [9]-[11]. However, the photocatalytic process of both TiO_2 and ZnO photocatalysts can only be activated under UV exposure owing to their wide band gap materials [12]. Meanwhile, a major challenge in photocatalysis is the recombination of electron-hole pairs, which limits photocatalytic degradation. To improve photocatalyst efficiency, several strategies have been investigated, such as the development of more stable catalysts through advanced synthesis techniques and the addition of materials in composite forms.

A simple and cost-effective method to enhance photocatalytic efficiency involves the application of mechanical force, for example, vibration or stirring, which helps keep catalyst particles in motion and separated. This approach, known as piezo-photocatalysis, combines photocatalysis with piezoelectric effects to convert mechanical energy into internal electrical potential to facilitate chemical reactions [13]. The generated internal electric field effectively separates the electron-hole pairs during light exposure, thereby reducing recombination and enhancing degradation performances. This technique not only accelerates the reaction but is also environmentally friendly, as it utilizes clean energy and produces no additional pollution. Nevertheless, conventional chemical wastewater treatments can be costly and may result in significant sludge formation or introduce toxic by-products. Moreover, the piezoelectric-enhanced photocatalytic process has been investigated in conjunction with ultrasound-assisted and sonophotocatalysis [14]. Piezoelectric materials with non-centrosymmetric structures respond to mechanical vibrations by generating internal electric fields through external deformation. These internal fields promote the separation of photogenerated charge carriers, thereby enhancing electrochemical and photochemical behaviors, and ultimately improving photocatalytic efficiency [15]. Promising piezo-photocatalytic materials such as zinc oxide [16], barium titanate ($BaTiO_3$) [17], bismuth-based compounds [18], and transition metal sulfides [19] exhibit both piezoelectric and photocatalytic properties when exposed to light irradiation combined with ultrasonic vibration. In particular, ZnO material possesses a non-centrosymmetric structure that contributes to its strong piezoelectric behavior and high responsivity in photocatalytic reactions. Due to these excellent properties, ZnO nanosheets have been shown to directly degrade steroid hormones under solar illumination coupled with mechanical stimulation by ultrasound waves [20]. Additionally, in Ag_2O/tetrapod-ZnO nanostructures, the separation of photogenerated electron–hole pairs can be facilitated by the built-in electric field at the heterojunction interface when subjected to ultrasonic and UV irradiation [21]. This process reduces the charge recombination rate and enhances photocatalytic activity for degrading organic pollutants in a piezo-assisted environment. Furthermore, ZnO hollow pitchfork structures have also been proposed for use in coupled photo-piezocatalytic systems targeting the removal of antibiotics and pesticides [22]. In the system, mechanical strain induces a piezo potential in the ZnO pitchfork, generating a polarized electric field that promotes photogenerated charge separation, significantly improving photocatalytic performance. Thus, a more effective and economical wastewater treatment process that incorporates the piezophototronic effect in photocatalysis is proposed. This method aims to produce efficient and cost-effective minimal sludges and ensure that the treated water meets environmental discharge standards [23]. Meanwhile, the unique morphology of ZnO nanostructures is particularly promising for piezo-photocatalytic applications for two main reasons: (i) their large specific surface area, which enhances photocatalytic activity, and (ii) their structural suitability for effectively responding to mechanical stimulation from ultrasound waves. Therefore, in this study, various ZnO nanostructures with spherical, plate-like, and rod-like morphologies were investigated as piezo-photocatalysts under xenon light irradiation with piezo-mechanical stimulation.

2. Experimental

ZnO nanostructures with rod-like and plate-like morphologies were synthesized via a one-step sol-gel method, as reported in our previous work [24]. Spherical ZnO powder was prepared following the method in Naik's work [25]. The crystalline structures and surface morphology of ZnO powders were characterized using X-ray diffraction (XRD; Rigaku SmartLab) and field emission scanning electron microscopy (FE-SEM; JEM-2100plus). Optical property in reflection mode was analyzed by UV-Vis-NIR spectroscopy (HITACHI-UH1450). For photocatalytic efficiency testing, a 10 µM RhB solution was used as a model dye pollutant. This solution was mixed with 0.003 g of ZnO samples and stirred in the dark for 30 minutes to establish adsorption equilibrium. The photocatalytic and piezocatalytic experiments were carried out under four different conditions: **CON 1:** stirring under light irradiation, **CON 2:** stirring in the absence of light, **CON 3:** piezo-assisted activation combined with light irradiation, and **CON 4:** piezo-mechanical activation in the dark. A xenon lamp was chosen as a light source (300 W) for 90 minutes, while the piezo-mechanical force was introduced using an ultrasonic bath. Absorbance measurements of the dye solutions were taken every 15 minutes using a UV-visible spectrophotometer (Heλios-UV6 123304).

3. Result and discussion

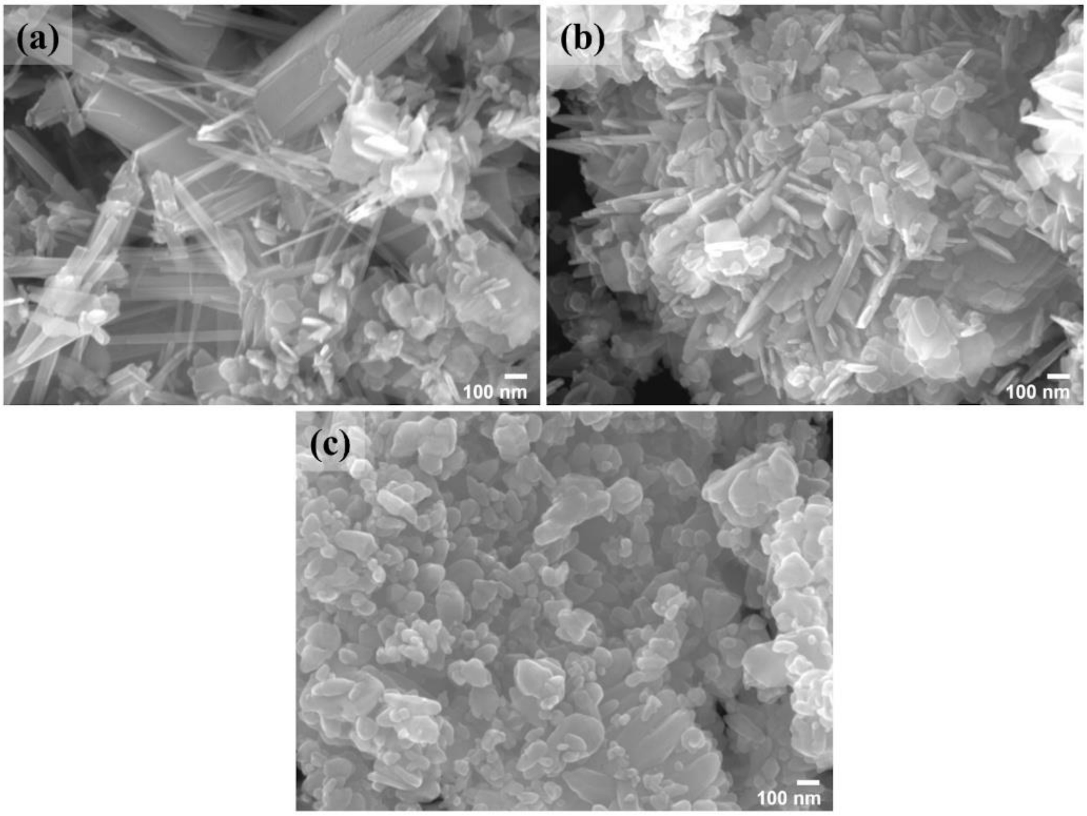

Fig. 1. FE-SEM images of ZnO nanostructures in a) rod-like, b) plate-like, and c) spherical shapes.

FE-SEM images at 20,000× magnification of ZnO nanostructures with rod-like, plated, and spherical morphologies are shown in Fig. 1. ZnO powder in rod-like structure, depicted in Fig. 1(a), exhibited a mixture of small rods and plate-like particles arranged in a disordered pattern, with some agglomerated clusters. The average size of ZnO nanorods was approximately 169 nm. Meanwhile, the plate-like ZnO in Fig. 1(b) displayed overlapping, flower-shaped structures, with noticeable aggregation in some regions and lower particle density in others. The average size of the plate-like particles was approximately 144 nm. Fig. 1(c) revealed numerous small spherical particles that tend to cluster in several areas, with an average particle size of approximately 158 nm. Variations in ZnO morphologies may be attributed to differences in synthesis parameters such as temperature, pH, and precursor materials [26]. Rod-shaped ZnO is typically synthesized using zinc acetate as the precursor, assisted by a one-step hydrothermal process, which is commonly employed to achieve this morphology due to the stronger basic solution compared to other precursors. Plate-like ZnO is generally synthesized using zinc sulfate, owing to the negligible basicity of SO_4^{2-} ions, which influences crystal growth and shape [24]. Spherical ZnO can also be synthesized using zinc acetate precursor. However, differences in the synthesis method and temperature, compared to the rod-like structure, lead to the formation of spherical particles [27].

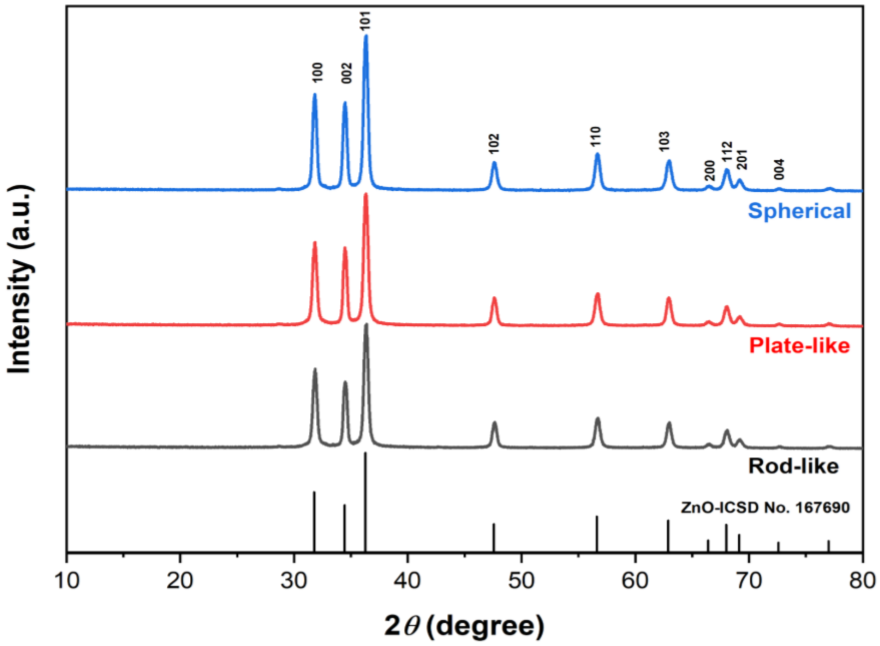

Fig. 2. XRD patterns of ZnO powder with different morphologies.

The crystal structures of ZnO with different morphologies was analyzed using XRD patterns over a 2θ range of 10°-80°, as depicted in Fig. 2. All ZnO samples exhibited similar diffraction patterns, characterized by the three prominent peaks corresponding to the (100), (002), (101), (102), (110), (103), (200), (112), (201), and (004) planes of hexagonal wurtzite structure, located at 2θ values of 31.8°, 34.4°, 36.3°, 47.6°, 56.6°, 62.9°, 66.4°, 68.0°, 69.1°, and 72.6°, respectively. No secondary or contaminated phases were detected, indicating high purity of the synthesized samples [28]. Furthermore, the average crystallite size (D) of the ZnO samples was calculated from the three main diffraction peaks using the Scherrer equation (Eq. 1) [29]:

$$D = \frac{k\lambda}{\beta cos\theta} \tag{1}$$

where, D is the average crystallite size,

k is the form factor (0.9),

λ is the wavelength of Cu Kα radiation (0.154 nm),

β is the width evaluated at mid-high of the most intense diffraction peak, and

θ is the Bragg angle.

The calculated average crystallite size of all ZnO samples, as presented in Table 1, was approximately 61, 59, and 56 nm for rod-like, plate-like, and spherical shapes. These values indicate that the crystallite sizes across all three morphologies are relatively similar, suggesting a similar ZnO crystal structure regardless of shape [30].

Table 1. The calculations of crystallite size and band gap energy in the different ZnO nanostructures.

ZnO morphologies	Crystallite size (nm)	Band gap energy (eV)
Rod-like	61	3.30
Plate-like	59	3.29
Spherical	56	3.25

The optical property of the ZnO samples using diffuse reflectance is illustrated in Fig. 3. The reflectance spectra of ZnO powders with three distinct morphologies were recorded in the range of 200-800 nm to assess their photocatalytic potential of light activation. In the UV region (200-400 nm), all ZnO samples showed negligible reflectance, indicating strong UV absorption irrespective of morphology [31]. Beyond 400 nm, the reflectance of all samples increased significantly, suggesting that ZnO reflected visible light effectively. This implies that ZnO materials are primarily active under UV irradiation, while visible light is mostly reflected and ineffective in initiating photocatalytic processes. However, since the light source used in this study is a xenon lamp, which emits both UV and visible light, the UV component is sufficient to activate the ZnO samples in photocatalytic activity. To estimate the band gap energy of ZnO samples, the Kubelka-Munk function was applied, as given by Eq. 2 [32]:

$$F(R) = \frac{(1-R)^2}{2R} \tag{2}$$

where *F(R)* is the Kubelka-Munk function and *R* is the reflectance value. Based on this analysis, the band gap energies of rod-, plate-, and spherical-shaped ZnO powders were found to range from 3.25-3.30 eV, as presented in Table 1. These values are slightly lower than the typical band gap of bulk ZnO, which is approximately 3.37 eV. Although the overall reflectance spectra of the samples show similar trends, minor differences are observed in the absorption edge. These variations can be attributed to differences in particle size, which influence light scattering across various wavelengths. Additionally, the shape and reduced size of ZnO particles can affect both light scattering and reflection, thereby corresponding to the tuning of band gap energy [33].

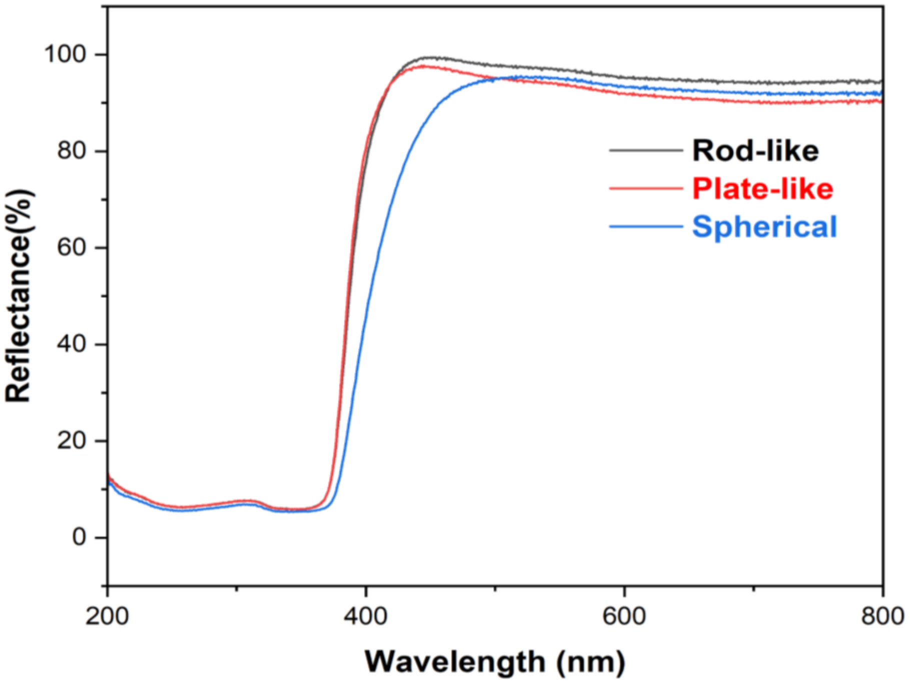

Fig. 3. Diffuse reflectance spectra of ZnO powder with different morphologies.

The analysis of RhB absorbance using rod-like ZnO photocatalysts under different photocatalytic activity is presented in Fig. 4 as follows: CON 1: stirring with light irradiation, CON 2: stirring in the absence of light, CON 3: ultrasonic treatment combined with light irradiation, and CON 4: ultrasonic treatment in the dark. Among these conditions, the most effective dye degradation occurred under CON 3, where the photocatalytic reaction was assisted with ultrasonic treatment. Normally, when ZnO photocatalyst is exposed to light with energy greater than its band gap, electron-hole pairs are generated. These charge carriers subsequently react with adsorbed oxygen and water molecules on the catalyst surface, producing superoxide radicals (O_2^{-}) and hydroxyl radicals ($OH^{\bullet}$) [34]. Moreover, the enhanced degradation observed under CON 3 is attributed to mechanical strain on the ZnO surface, which is associated with the generation of a piezoelectric potential. When combined with photocatalysis, an internal electric field induced by mechanical stress from the ultrasonic system can be generated, resulting in enhancing the photogeneration of electron-hole pairs [28]. This mechanism significantly improves photocatalytic efficiency by suppressing electron-hole pair recombination in a piezo-assisted environment. In the case of CON 1, this condition represents a conventional photocatalytic reaction. Rod-like ZnO demonstrates superior photocatalytic performance due to its entangled structure and large surface area, which provides more active sites for interaction with the surrounding aqueous solution [35]. In contrast, minimal dye degradation is observed under dark conditions in CON 2 (stirring only) and CON 4 (ultrasonication only), as the absence of sufficient light prevents activation on the photocatalyst surface. These results emphasize the essential role of light irradiation in the photocatalytic process. However, the decrease in dye absorbance observed in CON 2 is attributed to the efficient adsorption of dye molecules onto the ZnO surface from the aqueous environment [36]. Meanwhile, the higher degradation efficiency observed in CON 4, which involves ultrasonication alone, can be attributed to the formation of the acoustic cavitation process characterized by intense physical effects. When the intensity of ultrasonic waves exceeds the tensile strength of the medium, it disrupts the intermolecular structure, leading to the destabilization and breakdown of molecular integrity [37]. Therefore, the improvement of photocatalytic efficiency can be attributed to the piezoelectric effect, which arises from the non-centrosymmetric structure of the photocatalysts.

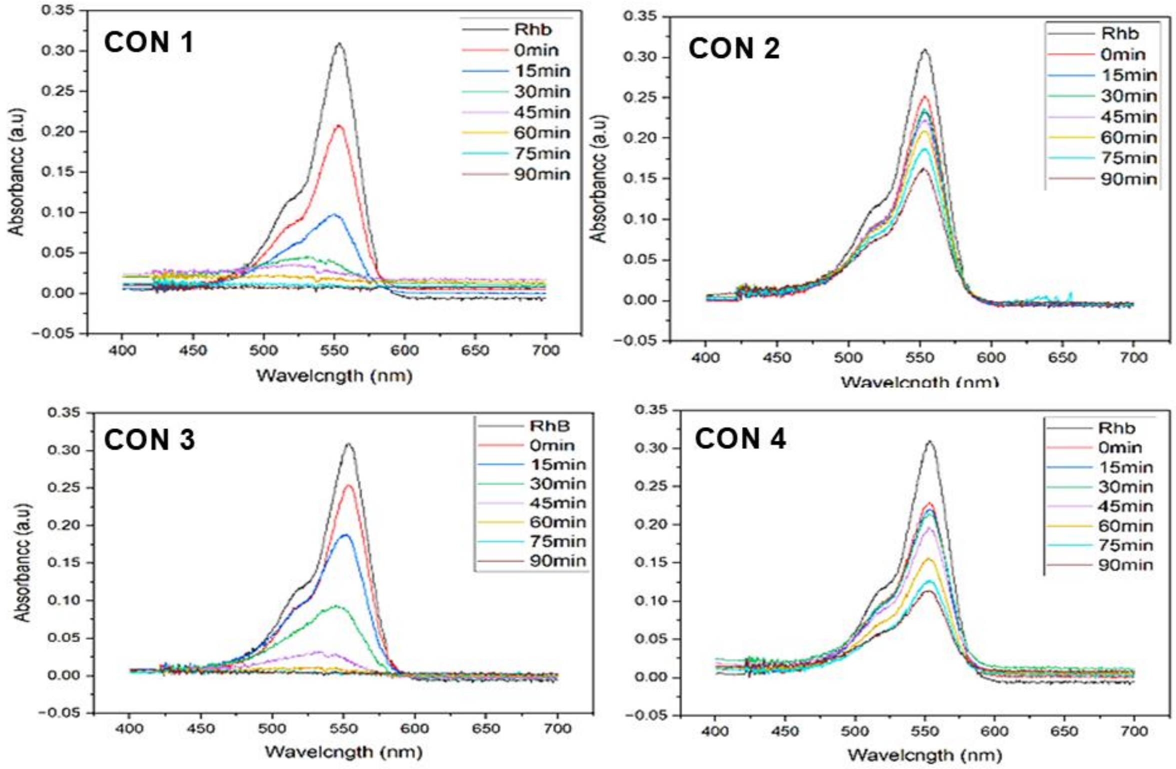

Fig. 4. Absorbance spectra of RhB solutions by rod-like ZnO photocatalysts under various photocatalytic environments.

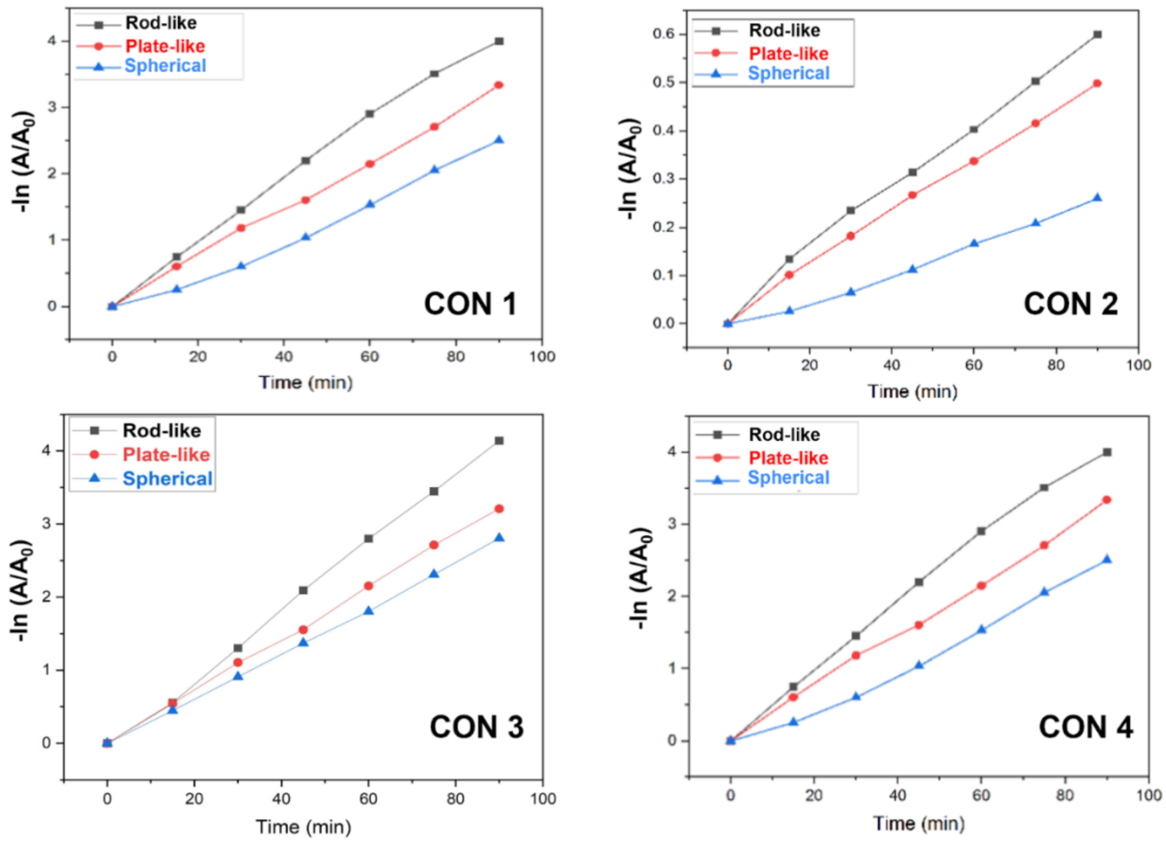

Fig. 5. The determination of the reaction rate by ZnO photocatalysts with different morphologies under various photocatalytic conditions.

Among the different ZnO structures tested, the rod-shaped morphology exhibits the highest degradation efficiency, followed by the plate-like and then the spherical form, as shown in Fig. 5. This evaluation is based on the specific absorption wavelength of rhodamine B, with its maximum absorption peak at 554 nm to determine the reaction rate (*k*). Over time, the absorbance spectra become increasingly linear, indicating a consistent decline in dye concentration and an increase in degradation rate with prolonged irradiation. Besides CON 3 with the combination of light and piezo irradiation showing the highest degradation efficiency, CON 1 in the standard photocatalytic reaction also yields effective degradation, emphasizing the importance of light in activating the photocatalytic process. In contrast, under dark conditions (CON 2 and CON 4), negligible RhB degradation occurs, indicating that photocatalytic activity requires light activation. Even in the presence of a catalyst, no significant photocatalytic reaction occurs without illumination [38]. The degradation rates under different photocatalytic conditions for various ZnO morphologies are summarized in Table 2. A first-order kinetic model is applied to evaluate the dye degradation rate at any given time, which is directly proportional to the remaining dye concentration. The kinetic equation used is as follows [39]:

$$ln\frac{A}{A_0} = -kt \tag{3}$$

where A is the dye absorbance at a given time,
A_0 is the initial dye absorbance (after equilibrium reaction),
k is the rate constant, indicating the reaction rate, and
t is the irradiation time (minutes).

The rate constant, k, is determined from the slope of the linear plot as depicted in Fig. 5. A higher k value indicates a more efficient ZnO photocatalyst under the dye degradation process. The logarithmic value of the ratio of dye absorbance before/after photocatalytic reaction on the Y-axis indicates the decrease in its absorbance during the prolonged irradiation time corresponding to the degradation of dye molecules under the photocatalytic reaction. This result confirms that the CON 3 involving ultrasonic treatment combined with light irradiation provides the highest dye degradation across all ZnO morphologies. The order of dye degradation efficiency for the morphologies in this condition was as follows: rod-shaped > plate-shaped > spherical-shaped ZnO. The highest dye degradation using rod-shaped ZnO was observed under CON 3. The presence of a rod-like ZnO photocatalyst demonstrates superior dye degradation performance, supported by the piezo-mechanical force generated from its non-centrosymmetric structure, which induces an internal electric field on the surface. Additionally, the rod-shaped structure also facilitates electron transport during the photocatalytic reaction owing to the directed pathways for electron transfer along its long axis [40]. These phenomena can be attributed to enhanced carrier photogeneration and the suppression of electron-hole recombination, which together promote a sustained photocatalytic reaction. Moreover, the high specific surface area to volume ratio of the plate-like structure plays a crucial role in photocatalytic activity. These morphologies provide a larger surface area, allowing more dye molecules to interact with a greater number of active sites on the catalyst surface compared to a spherical structure [41]. The photocatalytic efficiency of spherical ZnO is the lowest among all ZnO samples, which can be ascribed to its isotropic morphology and multi-directional electron paths. This structure tends to exhibit a weaker piezoelectric response under mechanical stimulation and leads to an increase in surface electron scattering compared to anisotropic morphologies. Additionally, ZnO nanoparticles commonly face agglomeration, driven by strong van der Waals forces and high surface energy. This agglomeration not only reduces the effective area but also promotes charge recombination and hinders efficient photogeneration, thereby significantly impairing their photocatalytic performance [42].

Table 2. The determination of *K* rate under different photocatalytic environments by various ZnO morphologies.

Photocatalytic environments	ZnO morphologies	*K* rate (min^{-1})
CON 1: Stirring under light irradiation	Rod-like	0.045
	Plate-like	0.036
	Spherical	0.028
CON 2: Stirring in the absence of light	Rod-like	0.003
	Plate-like	0.002
	Spherical	0.002
CON 3: A combination of piezo-assisted activation and light irradiation	Rod-like	0.046
	Plate-like	0.035
	Spherical	0.031
CON 4: Piezo-mechanical activation in the dark	Rod-like	0.006
	Plate-like	0.005
	Spherical	0.002

The percentage degradation of Rhodamine B dye using zinc oxide photocatalysts in different morphologies and under varying experimental conditions is illustrated in Fig. 6. Under CON 3 — the combination of ultrasonic irradiation and light exposure — the rod-shaped ZnO demonstrated the highest degradation efficiency at 98%, followed by the plate-shaped ZnO at 96%, and the spherical ZnO at 94% for 90 minutes. This evaluation confirms that the rod-shaped morphology exhibits the highest photocatalytic degradation efficiency. The second-best performance was observed in CON 1, which involved stirring with light irradiation, yielding a high percentage degradation of rod-like ZnO, approximately 96%. Meanwhile, the percentage degradation in CON 2 and CON 4 was slow due to the absence of light. However, the high degradation performance in CON 4 was higher than CON 2 owing to the influence of the interval electrical field under piezo-mechanical force. These results indicate that increasing reaction time leads to a corresponding decrease in dye concentration, affirming that piezo-assisted light irradiation conditions and ZnO morphology significantly influence photocatalytic performance. Specifically, rod-like morphologies with higher surface area enable more effective interactions between the dye molecules and the photocatalyst surface, thereby enhancing the photocatalytic degradation efficiency of RhB.

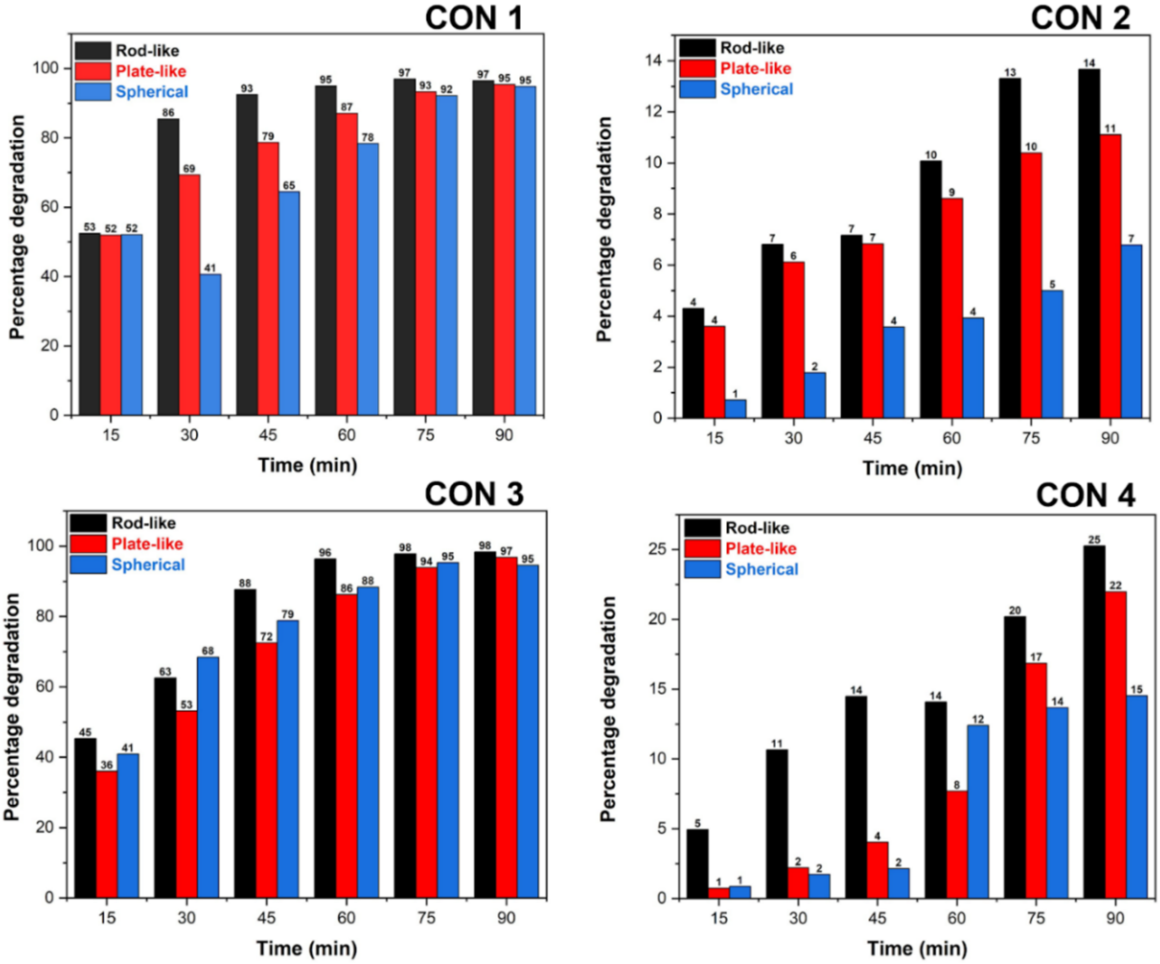

Fig. 6. The percentage degradation of RhB by ZnO photocatalysts with different morphologies under various photocatalytic conditions.

4. Conclusion

In this work, different ZnO morphologies were investigated for their piezo-photocatalytic properties. XRD patterns and SEM images confirmed that the synthesized ZnO powders—rod-like, plate-like, and spherical—corresponded to a hexagonal wurtzite crystal structure. DRS spectra indicated that all ZnO morphologies exhibited strong absorption in the ultraviolet region, with band gap energies ranging from approximately 3.25 to 3.30 eV. Among the tested samples, the rod-like ZnO photocatalyst under CON 3 (ultrasonic waves combined with light irradiation) achieved the most effective in dye degradation efficiency, with a reaction rate of 0.046 min^{-1}. This enhanced photocatalytic efficiency is attributed to the initial built-in electric potential generated by the mechanical strain due to the piezoelectric properties in ZnO. The asymmetric rod-like structure plays a key role in promoting effective electron-hole pair separation and facilitating charge photogeneration, thereby improving overall performance. Under Condition 1, which involved only light irradiation, the system operated as a conventional photocatalytic process and also exhibited the second-highest performance. In contrast, negligible RhB degradation was observed under stirring and ultrasonication only in CON 2 and CON 4, confirming that light activation is essential for initiating photocatalytic activity. However, CON 4 with ultrasonication alone showed a minor degree of dye degradation due to the intense physical effect of acoustic cavitation, which can lead to partial destabilization and breakdown of dye molecules. Regarding ZnO morphology, the rod-like structure demonstrated the highest photocatalytic performance, likely due to its larger crystal size and anisotropic geometry, which enhanced its piezoelectric response. The plate-like ZnO also showed promising results, with its high specific surface area and light-trapping ability, which contributed to increasing optical absorption and a greater number of active sites for dye interaction. Meanwhile, spherical ZnO photocatalyst showed reasonable performance in both piezo-assisted and conventional photocatalysis. Its isotropic morphology resulted in a weaker piezoelectric response under mechanical stimulation, limiting its effectiveness in the piezo-photocatalytic applications.

Acknowledgments

The Research on “Enhanced Piezo-Photocatalytic Degradation of Rhodamine B Using Different ZnO Nanostructures Under Xenon Irradiation and Ultrasonic Activation (Grant No. RE-KRIS/FF68/34) by King Mongkut’s Institute of Technology Ladkrabang (KMITL) has received funding support from the NSRF. The facility and analytical instruments were kindly provided by the Department of Nanoscience and Nanotechnology, School of Integrated Innovative Technology, KMITL, and Japan-ASEAN Science, Technology and Innovation Platform (JASTIP).

References

[1] Rad, S. M., Ray, A. K., & Barghi, S. (2022). Water Pollution and Agriculture Pesticide. *Clean Technologies*, *4*(4), 1088-1102. DOI: 10.3390/cleantechnol4040066.

[2] Gupta, V. K., Ali, I., Saleh, T. A., Nayak, A., & Agarwal, S. (2012). Chemical Treatment Technologies for Waste-water Recycling-an Overview. *RSC Advances*, *2*(16), 6380-6388. DOI: 10.1039/c2ra20340e.

[3] Metin, S., & Çifçi, D. İ. (2023). Chemical industry wastewater treatment by coagulation combined with Fenton and photo-Fenton processes. *Journal of Chemical Technology & Biotechnology*, *98*(5), 1158-1165. DOI: 10.1002/jctb.7321.

[4] Pavel, M., Anastasescu, C., State, R. N., Vasile, A., Papa, F., & Balint, I. (2023). Photocatalytic degradation of organic and inorganic pollutants to harmless end products: Assessment of practical application potential for water and air cleaning. *Catalysts*, *13*(2), 380. DOI: 10.3390/catal13020 380.

[5] Al-Nuaim, M. A., Alwasiti, A. A., & Shnain, Z. Y. (2023). The photocatalytic process in the treatment of polluted water. *Chemicke Zvesti*, *77*(2), 677-701. DOI: 10.1007/s11696-022-02468-7.

[6] Dharma, H. N. C, Jaafar, J., Widiastuti, N., Matsuyama, H., Rajabsadeh, S., Othman, M. H. D., Rahman, M. A., Jafri, N. N. M., Suhaimin N. S., Nasir A. M., & Alias N. H. (2022). A review of titanium dioxide (TiO_2)-based photocatalyst for oilfield-produced water treatment. *Membranes*, *12*(3), 345. DOI: 10.3390/membranes12030345.

[7] Zhu, C., & Wang, X. (2025). Nanomaterial ZnO synthesis and its photocatalytic applications: A review. *Nanomaterials*, *15*(9), 682. DOI: 10.3390/nano15090682.

[8] Ma, H., Hao, B., Song, W., Guo, J., Li, M., & Zhang, L. (2021). A high-efficiency TiO_2/ZnO nano-film with surface oxygen vacancies for dye degradation. *Materials*, *14*(12), 3299. DOI: 10.3390/ma14123299.

[9] Nazim, V. S., El-Sayed, G. M., Amer, S. M., & Nadim, A. H. (2023). Optimization of metal dopant effect on ZnO nanoparticles for enhanced visible LED photocatalytic degradation of citalopram: comparative study and application to pharmaceutical cleaning validation. *Sustainable Environment Research*, *33*(1), 39. DOI: 10.1186/s42834-023-00198-3.

[10] Mourya, A. K., Singh, R. P., Kumar, T., Talmale, A. S., Gaikwad, G.S., & Wankhade, A. V. (2023). Tuning the morphologies of ZnO for enhanced photocatalytic activity. *Inorganic Chemistry Communications*, *154*, 110850. DOI: 10.1016/j.inoche.2023.110850.

[11] Zhang, D., Liu, Z., & Mou, R. (2022). Preparation and characterization of WO_3/ZnO composite photocatalyst and its application for degradation of oxytetracycline in aqueous solution. *Inorganic Chemistry Communications*, *142*, 109667. DOI: 10.1016/j.inoche.2022.109667.

[12] Mohamadpour, F. & Amani, A. M. (2024). Photocatalytic systems: reactions, mechanism, and applications. *RSC Advances*, 14(29), 20609-20645. DOI: 10.1039/d4ra03259d.

[13] Su, X., Zhao, X., Cui, C., Xi, N., Zhang, X. L., Liu, H., Yu, X., & Sang, Y. (2022). Influence of wurtzite ZnO morphology on piezophototronic effect in photocatalysis. *Catalysts*, *12*(9), 946. DOI: 10.3390/catal12090946.

[14] Li, C., Wang, X., Wu, J., Gao, J., Zhao, R., Xia, S., Yang, H., Chen, Z., & Wang, W. (2023). Harnessing ultrasound in photocatalysis: Synthesis and piezo-enhanced effect: A review. *Ultrasonics Sonochemistry*, *99*, 106584. DOI: 10.1016/j.ultsonch.2023.106584.

[15] Jiang, Z., Tan, X., & Huang, Y. (2022). Piezoelectric effect enhanced photocatalysis in environmental remediation: State-of-the-art techniques and future scenarios. *Science of The Total Environment*, *806*, 150924. DOI: 10.1016/j.scitotenv.2021.150924.

[16] Li, T., Hu, W., Tang, C., Zhou, Z., Wang, Z., & Shu, L., (2023). Enhanced piezo-catalysis in ZnO rods with built-in nanopores. *Journal of Advanced Ceramics*, *12*(12), 2271-2283. DOI: 10.26599/jac.2023.9220819.

[17] Wan, L., Han, J., Tian, W., Li, N., Chen, D., & Lu, J., (2023). Barium titanate@covalent organic framework core-shell nanoparticles for adsorption-enhanced piezo-photocatalysis. *Chemical Engineering Journal*, *462*, 142324. DOI: 10.1016/j.cej.2023.142324.

[18] Wang, H., Zhang, X., Hu, C., Cai, H., Tu, S., & Huang, H., (2024). Layered perovskite piezoelectric Bi_3TiNbO_9 as a piezo-photocatalyst: Synergistically enhanced catalytic activity and mechanism. *Applied Surface Science*, *650*, 159214. DOI: 10.1016/j.apsusc.2023.159214.

[19] Zhang, Y., Wang, L., Huang, H., Hu, C., Zhang, X., Wang, C., & Zhang, Y., (2023). Water flow induced piezoelectric polarization and sulfur vacancy boosting photocatalytic hydrogen peroxide evolution of cadmium sulfide nanorods. *Applied Catalysis B: Environmental*, *331*, 122714. DOI: 10.1016/j.apcatb.2023.122714.

[20] Bettini, S., Pagano, R., Valli, D., Ingrosso, C., Roeffaers, M., Hofkens, J., Giancane, G., & Valli, L., (2023). ZnO nanostructures based piezo-photocatalytic degradation enhancement of steroid hormones. *Surfaces and Interfaces*, *36*, 102581. DOI: 10.1016/j.surfin.2022.102581.

[21] Sun, C., Fu, Y., Wang, Q., Xing, L., Liu, B., & Xue, X. (2016). Ultrafast piezo-photocatalytic degradation of organic pollutions by Ag_2O/tetrapod-ZnO nanostructures under ultrasonic/UV exposure. *RSC Advances*, *6*(90), 87446-87453. DOI: 10.1039/c6ra13464e.

[22] Sharma, A., Bhardwaj, U., & Kushwaha, H. S. (2022). ZnO hollow pitchfork: coupled photo-piezocatalytic mechanism for antibiotic and pesticide elimination. *Catalysis Science & Technology*, *12*(3), 812-822. DOI: 10.1039/D1CY01973B.

[23] Jing, L., Xu, Y., Xie, M., Li, Z., Wu, C., Zhao, H., Wang, J., Wang, H., Yan, Y., Zhong, N., Li, H., & Hu, J. (2023). Piezo-photocatalysts in the field of energy and environment: Designs, applications, and prospects. *Nano Energy*, *112*, 108508. DOI: 10.1016/j.nanoen.2023.108508.

[24] Songpanit, M., Boonyarattanakalin, K., Pecharapa, W., & Mekprasart, W. (2024). ZnO nanostructures synthesized by one-step sol-gel process using different zinc precursors. *Journal of Metals, Materials and Minerals*, *34*(3), 1968. DOI: 10.55713/jmmm.v34i3.1968.

[25] Naik, E. I., Naik, H. S. B., Sarvajith, M. S., & Pradeepa, E. (2021). Co-precipitation synthesis of cobalt doped ZnO nanoparticles: Characterization and their applications for biosensing and antibacterial studies. *Inorganic Chemistry Communications*, *130*, 108678. DOI: 10.1016/j.inoche.2021.108678.

[26] Søndergaard, M. & Boejesen, E., Christensen, M., & Iversen, B. (2011). Size and morphology dependence of ZnO nanoparticles synthesized by a fast continuous flow hydrothermal method. *Crystal Growth & Design*, *11*(9), 4027-4033. DOI: 10.1021/cg200596c.

[27] Raha, S. & Ahmaruzzaman, M. (2022). ZnO nanostructured materials and their potential applications: progress, challenges and perspectives. *Nanoscale Advances*, *4*(8), 1868-1925. DOI: 10.1039/d1na00880c.

[28] Chimupala, Y., Phromma, C., Yimklan, S., Semakul, N., & Ruankham, P. (2020). Dye wastewater treatment enabled by piezo-enhanced photocatalysis of single-component ZnO nanoparticles. *RSC Advances*, *10*(48), 28567-28575. DOI:10.1039/d0ra04746e.

[29] Fatimah, S., Ragadhita, R., Al Husaeni, D. F., & Nandiyanto, A. (2021). How to calculate crystallite size from X-ray diffraction (XRD) using Scherrer method. *ASEAN Journal of Science and Engineering*, *2*(1), 65-76. DOI: 10.17509/ajse.v2i1.37647.

[30] Harun, N., S.M.N. Mydin, R. B., Sreekantan, S., Saharudin, K. A., Ling, K. Y., Basiron, N., Radhi, F., & Seeni, A. (2018). Shape-dependent antibacterial activity against Staphylococcus aureus of zinc oxide nanoparticles. *Malaysian Journal of Medicine and Health Sciences*, *14*, 141-146.

[31] Hamzah, Y., Febiola, A., Umar, L. & Salomo. (2024). optical, structural and morphological studies of ZnO nanoparticles synthesized using Terminalia catappa leaf extract. *Journal of Physics: Conference Series*, *2734*, 012035. DOI: 10.1088/1742-6596/2734/1/012035.

[32] Myrick, M. L., Simcock, M. N., Baranowski, M., Brooke, H., Morgan, S. L., & McCutcheon, J. N. (2011). The Kubelka-Munk diffuse reflectance formula revisited. *Applied Spectroscopy Reviews*, *46*(2), 140-165. DOI: 10.1080/05704928.2010.537004.

[33] Kumar, S. S., Rao, V. R., & Rao, G. N. (2022). Effect of morphology, crystallite size and optical band gap on photocatalytic activity of ZnO nanostructures for decolorization of R6G. *Materials Today: Proceedings*, *62*, 5494-5502. DOI: 10.1016/j.matpr.2022.04.220.

[34] Baig, A., Siddique, M., & Panchal, S. (2025). A review of visible-light-active zinc oxide photocatalysts for environmental application. *Catalysts*, *15*(2), 100. DOI: 10.3390/catal15020100.

[35] Rasheedi, A. A., Salwati, A., Ansari, A. R., Hassaneen, A. A. D., & Aida, M. S. (2023). Photocatalysis activity of ZnO nanorods arrays prepared via hydrothermal. *Inorganic Chemistry Communications*, *158*, 111568. DOI: 10.1016/j.inoche.2023.111568.

[36] Al-Arjan, W. S. (2022). Zinc oxide nanoparticles and their application in adsorption of toxic dye from aqueous solution. *Polymers*, *14*(15), 3086. DOI: 10.3390/polym14153086.

[37] Teh, C. Y., Wu, T. Y., & Juan, J. C. (2017). An application of ultrasound technology in synthesis of titania-based photocatalyst for degrading pollutant. *Chemical Engineering Journal*, *317*, 586-612. DOI: 10.1016/j.cej.2017.01.001.

[38] Hassaan, M. A., El-Nemr, M. A., Elkatory, M. R., Ragab, S., Niculescu, V. C., & Nemr A. E. (2023). Principles of photocatalysts and their different applications: A review. *Topics in Current Chemistry*, *381*(6), 31. DOI: 10.1007/s41061-023-00444-7.

[39] Tran, H. D., Nguyen, D. Q., Do, P. T., & Tran, U. N. P. (2023). Kinetics of photocatalytic degradation of organic compounds: a mini-review and new approach. *RSC Advances*, *13*(25), 16915-16925. DOI: 10.1039/d3ra01970e.

[40] Wibowo, A., Marsudi, M. A., Amal, M. I., Ananda, M. B., Stephanie, R., Ardy, H., & Diguna, L. J. (2020). ZnO nanostructured materials for emerging solar cell applications. *RSC Advances*, *10*(70), 42838-42859. DOI: 10.1039/d0ra07689a.

[41] Redjili, S., Ghodbane, H., Tahraoui, H., Abdelouahed, L., Chebli, D., Ola, M. S., Assadi, A. A., Kebir, M., Zhang, J., Amrane, A., & Lekmine, S. (2025). Green innovation: multifunctional zinc oxide nanoparticles synthesized using Quercus robur for photocatalytic performance, environmental, and antimicrobial applications. *Catalysts*, *15*(3), 256. DOI: 10.3390/catal15030256.

[42] Kumar, S. G., & Rao, K. S. R. K. (2015). Zinc oxide based photocatalysis: tailoring surface-bulk structure and related interfacial charge carrier dynamics for better environmental applications. *RSC Advances*, *5*(5), 3306-3351. DOI: 10.1039/c4ra13299h.